Inorg. Chem. **2008**, *47*, 11656−11668

Circular Dichroism of Trigonal Dihedral Chromium(III) Complexes: A Theoretical Study based on Open-Shell Time-Dependent Density Functional Theory

Jing Fan,[†] Michael Seth,[†] Jochen Autschbach,[‡] and Tom Ziegler*[,†]

Department of Chemistry, University of Calgary, Calgary, Alberta, Canada, T2N 1N4, and Department of Chemistry, University at Buffalo, State University of New York, 312 Natural Science Complexes, Buffalo, New York 14260-30000

Received July 2, 2008

Spin-unrestricted time-dependent density functional theory has been applied to the electronic circular dichroism spectra of Cr(III) complexes with an open-shell ground state, that is, $[Cr(L\text{-}L)_3]^{n+}$ with L-L = en(ethylenediamine), acac(acetylacetonate), ox(oxalate), mal(malonate), and Thiox(dithiooxalate). The simulated CD spectra are analyzed in details and compared with experimental data, as well as previous calculations on similar Co(III) complexes where available. The theoretical results serve as a tool for elucidating the absolute configuration of similar complexes, by pointing to transitions for which the sign of the rotatory strength can be used as fingerprint for one particular configuration.

1. Introduction

The measurement of electronic circular dichroism (CD)[1,2] has long been employed to determine the absolute configurations of chiral molecules. Theoretical work can greatly aid in the interpretation of such spectra and might further help in pointing out CD bands that can be used safely to determine the absolute configuration for a class of similar chiral molecules.

Time-dependent density functional theory (TD-DFT)[3,4] has become an important approach for the study of optical activity because of its accuracy and computational efficiency. Applications of TD-DFT to optical activity have been reported for a number of organic[5−10] compounds as well as transition metal complexes.[9−18] The reliability of the TD-DFT method and sources of errors has been assessed in detail.[6,13,15,19] All these studies have been confined to systems with a closed-shell ground state. Meanwhile, limited studies have been reported for electronic CD of open-shell transition metal complexes.[20,21] Excitation energies of some open-shell transition metal compounds have been investigated by us[22] and others.[23,24]

* To whom correspondence should be addressed. E-mail: ziegler@ucalgary.ca.
[†] University of Calgary.
[‡] University at Buffalo, State University of New York.

(1) *Fundamental aspects and recent developments in optical rotatory dispersion and circular dichroism*; Ciardelli, F., Salvadori, P., Eds.; Heyden & Son Ltd.: London, 1973.
(2) *Circular Dichroism: Principle and Applications*, 2nd ed.; Berova, N., Nakanishi, K., Woody, R. W., Eds.; Wiley-VCH: New York, 2000.
(3) Dobson, J. F. Time-dependent density functional theory. In *Electronic density functional theory. Recent progress and new directions*; Dobson, J. F., Vignale, G., Das, M. P., Eds.; Plenum Press: New York, 1998.
(4) Runge, E.; Gross, E. K. U. *Phys. Rev. Lett.* **1984**, *52*, 997–1000.
(5) McCann, D. M.; Stephens, P. J. *J. Org. Chem.* **2006**, *71*, 6074–6098.
(6) Autschbach, J.; Ziegler, T.; van Gisbergen, S. J. A.; Baerends, E. J. *J. Chem. Phys.* **2002**, *116*, 6930–6940.
(7) Tanaka, T.; Kodama, T. S.; Morita, H. E.; Ohno, T. *Chirality* **2006**, *18*, 652–661.
(8) Furche, F.; Ahlrichs, R.; Wachsmann, C.; Weber, E.; Sobanski, A.; Vogtle, F.; Grimme, S. *J. Amer. Chem. Soc.* **2000**, *122*, 1717–1724.
(9) Thulstrup, P. W.; Larsen, E. *Dalton Trans.* **2006**, *14*, 1784–1789.
(10) Autschbach, J.; Jensen, L.; Schatz, G. C.; Tse, Y. C. E.; Krykunov, M. *J. Phys. Chem. A* **2006**, *110*, 2461–2473.
(11) Jensen, L.; Swart, M.; Van Duijnen, P. T.; Autschbach, J. *Int. J. Quantum Chem.* **2006**, *106*, 2479–2488.
(12) Jorge, F. E.; Autschbach, J.; Ziegler, T. *J. Amer. Chem. Soc.* **2005**, *127*, 975–985.
(13) Guennic, B. L.; Hieringer, W.; Görling, A.; Autschbach, J. *J. Phys. Chem. A* **2005**, *109*, 4836–4846.
(14) Jorge, F. E.; Autschbach, J.; Ziegler, T. *Inorg. Chem.* **2003**, *42*, 8902–8910.
(15) Autschbach, J.; Jorge, F. E.; Ziegler, T. *Inorg. Chem.* **2003**, *42*, 2867–2877.
(16) Diedrich, C.; Grimme, S. *J. Phys. Chem. A* **2003**, *107*, 2524–2539.
(17) Bark, T.; Zelewsky, A. von.; Rappoport, D.; Neuburger, M.; Schaffner, S.; Lacour, J.; Jodry, J. *Chem.—Eur. J.* **2004**, *10*, 4839–4845.
(18) Coughlin, F. J.; Oyler, K. D.; Pascal, R. A., Jr.; Bernhard, S. *Inorg. Chem.* **2008**, *47*, 974–979.
(19) Autschbach, J. *Coord. Chem. Rev.* **2007**, *251*, 1796–1821.
(20) Vargas, A.; Zerara, M.; Krausz, E.; Hauser, A.; Daku, L. M. L. *J. Chem. Theor. Comput.* **2006**, *2*, 1342–1359.
(21) Pau, M. Y. M.; Davis, M. I.; Orville, A. M.; Lipscomb, J. D.; Solomon, E. I. *J. Amer. Chem. Soc.* **2007**, *129*, 1944–1958.

10.1021/ic801229c CCC: $40.75
Published on Web 11/14/2008

Experimentally, the optical activity of the complex ion $[Cr(en)_3]^{3+}$ has been studied extensively, with special attention given to the part of its low energy CD spectrum that is associated with spin-forbidden transitions.[25,26] Meanwhile, studies on Cr(III) complexes of relatively common ligands such as acetylacetonate, oxalate, or malonate, and so forth are limited and in some cases (e.g., $[Cr(mal)_3]^{3-}$) contradictory assignments of the absolute configuration have been reported.[27,28]

In the present work we report on the calculations of electronic CD spectra for some open-shell trigonal dihedral Cr(III) complexes by spin-unrestricted TD-DFT. Reasonable agreement between theory and experiment is achieved. The theoretical CD results are analyzed in details. We have further correlated the simulated CD spectra of the Cr(III) complexes with their Co(III) analogues to facilitate the interpretation of both systems.

2. Computational Details

The calculations have been carried out with a modified CD version of the Amsterdam density functional (ADF) program.[29−31] The ground-state of the open-shell systems are treated within DFT by a spin-unrestricted approach.[30] Frozen core-valence triple-ς polarized (TZP) Slater basis sets from the ADF database have been employed for all the calculations. The $1s^2$ shells on C, N, O and the $1s^22s^22p^6$ shells on S and Cr were taken as cores. In the TD-DFT calculations, we consider only the spin and symmetry allowed excitations. Rotatory strengths presented here are computed with the dipole-length formula. We found from test calculations that rotatory strengths with the dipole-velocity form were in good agreement with those obtained from the dipole-length formula. On the basis of the computed excitation energies and associated rotatory strengths, CD spectra have been simulated for comparison with experimental data. An empirical recipe[32] has been employed to simulate all the spectra, in which the bandwidth $\Delta\bar{\nu}$ is given by $\Delta\bar{\nu} = 7.5(\bar{\nu})^{1/2}$, where $\bar{\nu}$ is the absorption frequency in cm^{-1}. Numerical data for the experimental spectra have been extracted using the "g3data" software.[33] The simulated CD spectra are shifted (see figure caption for details) to facilitate the comparison with experiment. Errors arising from the functional, XC kernel, solvation, and so forth have been discussed in details.[13,15] The actual calculated transition energies are given in tables.

The "Conductor-like continuum Solvent MOdel" (COSMO)[34,35] has been applied in the calculations of the CD spectra to simulate solvent effects. The solvent used in both experimental and theoretical spectra is water unless stated otherwise. The TD-DFT calculations have been carried out based on optimized geometries. All the complexes are treated under D_3 symmetry constraint. The Vosko−Wilk−Nusair (VWN)[36] local density approximation (LDA) with the Becke88-Perdew86 (BP86) gradient corrections[37,38] has been used in all the CD calculations. The application of asymptotically correct XC potentials, for example, SAOP[39] and LB94,[40] did not improve the agreement of the simulated spectra with experiment. This observation is in line with our experience from previous studies on other systems.[20,22]

3. Results and Discussion

We shall in the following discuss results from calculations on the CD spectra of a number of trigonal dihedral Cr(III) d^3 complexes. Our findings will be compared with results from studies of similar Co(III) d^6 systems.[41] The simulated CD spectra for the complexes studied are displayed along with the experiment where available. For each system, the position of the computed excitation energies, as well as the sign and magnitude of each rotatory strength, are indicated by a bar spectrum. Transitions that are most important for the CD spectra are numbered and identified for detailed discussion. Some transitions of less importance are shown in the bar spectrum but not included in the numbering. The relevant spectral information is summarized in Tables as well. The experimental data were taken from the literature as follows: Λ-$[Cr(en)_3]^{3+}$,[42] Λ-$[Cr(ox)_3]^{3-}$ and Λ-$[Cr(mal)_3]^{3-}$,[27] Λ-$Cr(acac)_3$,[43] and Λ-$[Cr(Thiox)_3]^{3-}$.[44] In the case where the optical antipode of the complex was reported, the published experimental CD spectra have been inverted.

3.1. Tris(diamine) Complexes. $[M(en)_3]^{3+}$ (M = Cr, Co). We shall start with the ethylenediamine ligand, where only σ-type orbitals are involved in describing the ligand and its coordination to Cr(III). The corresponding $[Co(en)_3]^{3+}$ complex has been studied extensively.[15,45] It is well-known[46] that five-membered ethylenediamine rings in chelate complexes can adopt one of two enantiomeric conformations, depending on whether the C−C bond of the ring has a parallel (*lel*) or oblique (*ob*) orientation with respect to the C_3 axis of the complex. In practice, the energy difference between the two forms can be rather small and all conformers might be present in solution at room temperature. The X-ray studies[47] of crystals containing $[Cr(en)_3]^{3+}$ show the presence of lel_2ob, $lelob_2$, and ob_3 conformers of the complex cation

(22) Wang, F.; Ziegler, T. *Mol. Phys.* **2004**, *102*, 2585–2595.
(23) Nemykin, V. N.; Basu, P. *Inorg. Chem.* **2003**, *42*, 4046–4056.
(24) Cronstrand, P.; Rinkevicius, Z.; Luo, L.; Ågren, H. *J. Chem. Phys.* **2005**, *122*, 224104.
(25) Kaizaki, S.; Hidaka, J.; Shimura, Y. *Bull. Chem. Soc. Jpn.* **1970**, *43*, 1100–1109.
(26) Geiser, U.; Güdel, H. U. *Inorg. Chem.* **1981**, *20*, 3013–3019.
(27) McCaffery, A. J.; Mason, S. F.; Ballard, R. E. *J. Chem. Soc.* **1965**, 2883–2892.
(28) Butler, K. R.; Snow, M. R. *J. Chem. Soc., Dalton Trans.* **1976**, 251–258.
(29) Guennic, B. L.; Hieringer, W.; Görling, A.; Autschbach, J. *J. Phys. Chem. A* **2005**, *109*, 4836–4846.
(30) te Velde, G.; Bickelhaupt, F. M.; Baerends, E. J.; van Gisbergen, S. J. A.; Fonseca Guerra, C.; Snijders, J. G.; Ziegler, T. *J. Comput. Chem.* **2001**, *22*, 931–967.
(31) *Amsterdam Density Functional program*; Theoretical Chemistry, Vrije Universiteit: Amsterdam, 2008; URL: http://www.scm.com.
(32) Brown, A.; Kemp, C. M.; Mason, S. F. *J. Chem. Soc. A* **1971**, 751–755.
(33) Frantz, J. *g3data*, 2008; URL: http://beam.helsinki.fi/ frantz/software/g3data.php.
(34) Klamt, A.; Schüürmann, G. *J. Chem. Soc., Perkin Trans.* **2 1993**, 799–805.
(35) Pye, C. C.; Ziegler, T. *Theor. Chem. Acc.* **1999**, *101*, 396–408.
(36) Vosko, S. H.; Wilk, L.; Nusair, M. *Can. J. Phys.* **1980**, *58*, 1200–1211.
(37) Becke, A. D. *Phys. Rev. A* **1988**, *38*, 3098–3100.
(38) Perdew, J. P. *Phys. Rev. B* **1986**, *33*, 8822–8824.
(39) Schipper, P. R. T.; Gritsenko, O. V.; Van Gisbergen, S. J. A.; Baerends, E. J. *J. Chem. Phys.* **2000**, *112*, 1344–1352.
(40) Van Leeuwen, R.; Baerends, E. *J. Phys. Rev. A* **1994**, *49*, 2421–2431.
(41) Fan, J.; Ziegler, T. *Inorg. Chem.* **2008**, *47*, 4762–4773.
(42) Rancke-Madsen, M.; Woldbye, F. *Acta Chem. Scand.* **1972**, *26*, 3405–3412.
(43) Nordén, B. *Inorg. Nucl. Chem. Lett.* **1975**, *11*, 387–394.
(44) Hidaka, J.; Douglas, B. E. *Inorg. Chem.* **1964**, *3*, 1724–1728.
(45) Fan, J.; Ziegler, T. *Chirality* **2008**, *20*, 938–950.
(46) Corey, E. J.; Bailar, J. C. *J. Am. Chem. Soc.* **1959**, *81*, 2620–2629.

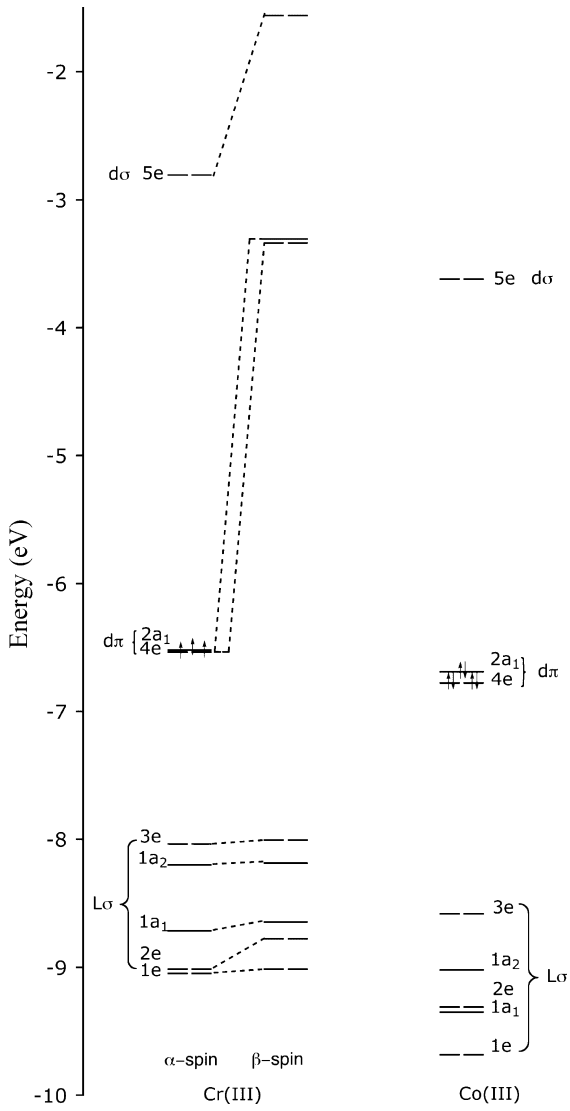

Figure 1. Molecular orbital diagram for $[M(en)_3]^{3+}$ (M = Cr, Co). In the Cr(III) case, the levels on the left are α-spin orbitals and those on the right are β-spin orbitals.

because of hydrogen bonding with the counteranion. It would be difficult to predict the most stable conformer in strongly hydrogen-bonding solvents, such as water.[47] In the present work, the *ob*$_3$-conformation of the Λ-$[Cr(en)_3]^{3+}$ ion is assumed to be dominant in solution, and all results presented in the following sections refer to calculations on this conformer. On the other hand, the *lel*-conformation of the Λ-$[Co(en)_3]^{3+}$ ion was observed in a number of crystals by X-ray studies.[48] Computational results presented here for this complex ion therefore refer to the *lel* conformer.

The orbital energy diagram for $[Cr(en)_3]^{3+}$ from spin-unrestricted DFT calculations is displayed in Figure 1 that shows the energies of both α- and β-spin orbitals. Under D_3 symmetry, the metal-based singly occupied molecular orbitals (SOMOs) of t_{2g} parentage (dπ) become the $2a_1$ and 4e orbitals. In our calculations, it is the α-based $2a_1$ and 4e MOs that are occupied. The fully unoccupied metal-based MOs

Scheme 1. Correlation of Energy Level Diagram for Lowest Excited States of Cr(III) and Co(III) Hexacoordinated Complexes in O_h and D_3 Symmetry

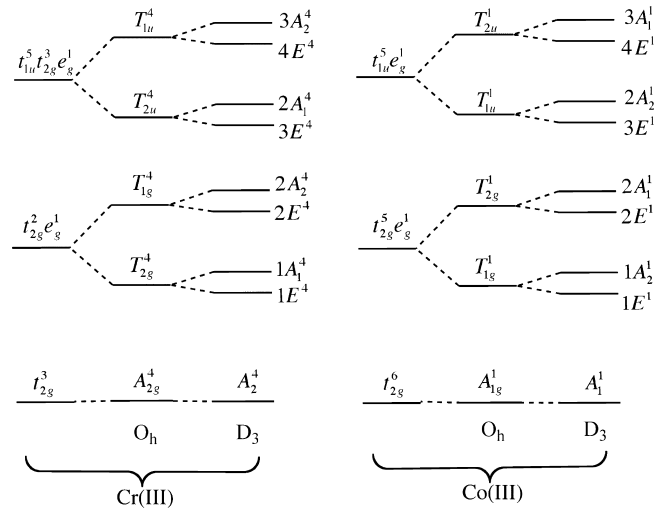

(dσ), resulting from the interaction between the metal e_g-set and the ligand σ-orbitals, appear as the 5e orbitals. The ligand σ-orbitals (Lσ) are fully occupied and situated below the dπ. We note that the α-levels with three excess electrons are lower in energy than the β-levels as the α-electrons undergo more exchange stabilization. The MO diagram of the cobalt analog is also presented in Figure 1. We see from the two diagrams in the figure that the dπ-dσ energy gap in the Cr(III) system as expected is larger than that in Co(III) since the more diffuse d-orbitals in Cr(III) have stronger interactions (overlaps) with the ligand orbitals. The energy level diagram arising from the splitting of O_h d^n states of Cr(III) and Co(III) in a trigonal field is shown in Scheme 1. In the present work, we consider only spin-allowed quartet-to-quartet transitions. In some cases, spin-unrestricted calculations can introduce spin contamination so that the result no longer represents transitions between pure spin states. Fortunately, it is less common to find significant spin contamination in DFT calculations, in comparison with unrestricted Hartree−Fock (UHF) and unrestricted Møller−Plesset (UMP) calculations.[49]

Although our objective in this work is the CD spectra of the Cr(III) systems, extensive comparison will also be made to the corresponding Co(III) systems. The experimental and simulated spectra for $[Cr(en)_3]^{3+}$ are given in Figure 2a and those for $[Co(en)_3]^{3+}$ in Figure 2b. In the following discussion, we label transitions that are common for Cr(III) and Co(III) systems with Arabic numbers as 1, 2, 3, and so forth according to the order in which they appear in the Cr(III) complexes. The Cr(III) compounds with a half-filled dπ shell have in addition a number of transitions that are not possible in the Co(III) complexes. These transitions are numbered x_1, x_2, and so forth in the order they appear.

In general, the low-energy part of the calculated spectra for d^6 $[M(en)_3]^{n+}$ complexes exhibit two transitions (1 and 2) with rotatory strengths of opposite sign. The two transitions 1(E) and 2(A_2) in $[Co(en)_3]^{3+}$ correspond to excitations

(47) Raymond, K. N.; Corfield, P. W. R.; Ibers, J. A. *Inorg. Chem.* **1968**, *7*, 842–844.
(48) Saito, Y. *Pure Appl. Chem.* **1968**, *17*, 21–36.
(49) Young, D. C. *Computational chemistry: a practical guide for applying techniques to real world problems*; Wiley: New York, 2001.
(50) Mason, S. F.; Seal, R. H. *Mol. Phys.* **1976**, *31*, 755–775.

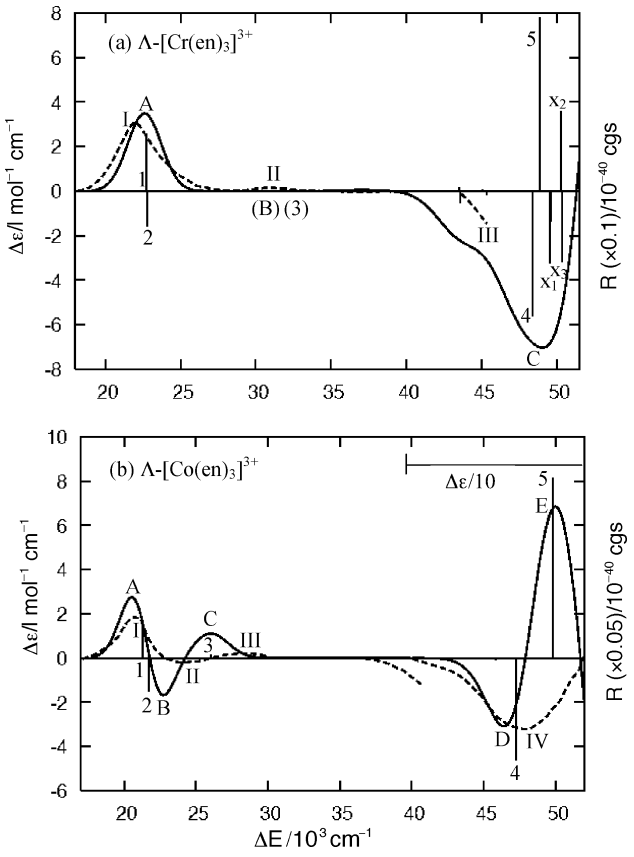

Figure 2. (a) Simulated (solid line) and experimental[42] (dashed line) CD spectra for Λ-$[Cr(en)_3]^{3+}$. The experimental spectrum is magnified by a factor of 2. Computed excitation energies smaller and larger than 40×10^3 cm^{-1} are shifted by -6.4×10^3 cm^{-1} and by $+6.0 \times 10^3$ cm^{-1}, respectively; (b) Simulated (solid line) and experimental[50] (dashed line) CD spectra for Λ-$[Co(en)_3]^{3+}$. Computed excitation energies smaller and larger than 40×10^3 cm^{-1} are shifted by -5.4×10^3 cm^{-1} and by $+6.0 \times 10^3$ cm^{-1}, respectively. Theoretical excitation energies and rotatory strengths are indicated by bars. The factor by which computed rotatory strengths are scaled is indicated in parenthesis. Bands in the experimental and simulated spectra are indicated by Roman numerals and by alphabetic letters, respectively.

to states of E and A_2 symmetry, and they constitute the d-to-d transition $A_{1g}{}^1 \rightarrow T_{1g}{}^1$ of O_h parentage. The bands corresponding to 1(E) and 2(A_2) in Figure 2b are given as A and B, respectively. The rotatory strength due to the sum of the contribution from the two degenerate E states is positive and larger in absolute terms than the negative rotatory strength from transition 2 due to the singly degenerate A_2 state, see Table 1 and Figure 2b. In the corresponding experimental spectrum[47] for $[Co(en)_3]^{3+}$ the bands I and II were assigned respectively to 1(E) and 2(A_2). At somewhat higher energy we find in the simulated spectrum of $[Co(en)_3]^{3+}$ another d-to-d excitation 3(E) corresponding to the $A_{1g}{}^1 \rightarrow T_{2g}{}^1$ transition of O_h parentage with a very weak CD band C. The same transition is seen in the experimental spectrum as the weak CD band III.

We find from our calculations on the analogous Λ-$[Cr(en)_3]^{3+}$ system in the d-to-d transition region two excitations 1(E) and 2(A_2) with respectively positive and negative rotatory strength as in the cobalt case. However, the two corresponding bands have collapsed into one band A because of the small splitting between 1 and 2, Figure 2a. The combined CD band A is positive as it is dominated by

Table 1. Spectral Properties for Λ-$[Cr(en)_3]^{3+}$

no.	R^a (10^{-40} cgs)	ΔE^b (10^3 cm^{-1})	symmetry[c]	one-electron excitation[d] MO→MO	%
1	+25.56	29.18	E	α: 4e → 5e	50
				α: $2a_1$ → 5e	49
2	−15.64	29.25	A_2	α: 4e → 5e	99
3	−5.52	37.60	E	β: 3e → 4e	99
4	−56.11	42.42	E	α: 3e → 5e	85
				α: $1a_2$ → 5e	12
5	+77.95	42.85	A_2	α: 3e → 5e	88
x_1	−32.26	43.58	A_2	β: 2e → 4e	93
x_2	+35.67	44.28	E	β: 2e → $2a_1$	58
				α: $1a_2$ → 5e	20
				β: 2e → 4e	17
x_3	−32.00	44.40	E	α: $1a_2$ → 5e	57
				β: 2e → 4e	14
				β: 2e → $2a_1$	10

[a] Rotatory strength; for the degenerate E states the rotatory strength given is the sum of the contribution from E_x and E_y. [b] Excitation energy. [c] Symmetry of the excited state. [d] Major contributions from one electron excitations to the transition.

the positive rotatory strength from 1(E). We find in the experimental spectrum in the same energy region a positive CD band designated "I" which we assign to the sum of the 1(E) and 2(A_2) excitations originating from the $A_{2g}{}^4 \rightarrow T_{2g}{}^4$ d-to-d transition of O_h parentage, Scheme 1. For $[Cr(en)_3]^{3+}$, there is as for $[Co(en)_3]^{3+}$ an excitation 3(E) with a corresponding positive CD band B now originating from the $A_{2g}{}^4 \rightarrow T_{1g}{}^4$ d-to-d transition of O_h parentage, Scheme 1. The rotatory strength for 3(E) is too small to be properly presented in Figure 2a. In the experimental spectrum of $[Cr(en)_3]^{3+}$, 3(E) is assigned to the weak positive band II.

The high-energy part of the simulated CD spectra for both complexes exhibits two CD active excitations 4(E) and 5(A_2), Table 1 and Figure 2, which correspond to the ligand-to-metal charge transfer (LMCT) transitions $A_{1g}{}^1 \rightarrow T_{1u}{}^1$ for the Co(III) system or $A_{2g}{}^4 \rightarrow T_{2u}{}^4$ for Cr(III). Both transitions can be described in O_h symmetry as an excitation from the t_{1u}(3e, $1a_2$) ligand levels to the e_g(5e) dσ metal levels. In $[Co(en)_3]^{3+}$, 4(E) and 5(A_2) are clearly separated in the simulated spectrum giving rise to the distinct negative band D and positive band E. Experimentally, the corresponding E component is designated IV. For the simulated CD of $[Cr(en)_3]^{3+}$, 4(E) and 5(A_2) are close in energy and they together with the other transitions x_1(A_2), x_2(E), and x_3(E) give rise to one negative band C. Here, x_1, x_2, and x_3 all have contributions from ligand orbitals ($1a_2$, 2e) to the empty dπ-orbitals (4e, $2a_1$) of t_{2g} parentage. Unfortunately, in the experiment only the onset of the band III containing the transitions 4, 5, and $x_{1,2,3}$ has been recorded as the start of a negative CD band. With modern techniques, it should be possible to obtain the whole band III.

For σ-bonded tris(bidentate) complexes, it has been shown[45,50,51] that the signs and the splitting of the two CD bands due to the $A_{1g}{}^1 \rightarrow T_{1g}{}^1$ parentage can be related respectively to the azimuthal and polar distortions of the octahedron formed by the six ligating atoms. Based on qualitative arguments[45] one can show that E(d-d) and A_2(d-d) should have respectively positive and negative rotatory

(51) Judkins, R. R.; Royer, D. J. *Inorg. Chem.* **1974**, *13*, 945–950.

Scheme 2. Orbital Interactions between $d\pi(a_1)$ and $L\sigma(a_1)$ for Different Polar Distortions

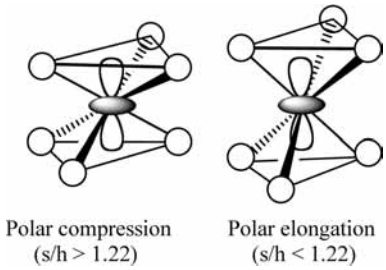

strength whereas E(LMCT) and A_2(LMCT) have respectively negative and positive rotatory strengths for the Λ-configuration with azimuthal angels (ϕ) less than 60° ($\Delta\phi < 0$, azimuthal contraction). All the signs are reversed for azimuthal angles larger than 60° ($\Delta\phi > 0$, azimuthal expansion). The same rules can be derived for the E(d-d) and A_1(d-d) as well as the E(LMCT) and A_1(LMCT) in the similar d^3 complexes. On the other hand, the sign of E-A_2 band split can be related to the polar distortion; $\upsilon(E) < \upsilon(A_2)$ for a polar compression (s/h > 1.22) along the C_3 axis and $\upsilon(E) > \upsilon(A_2)$ for an elongation (s/h < 1.22). The influence of the polar distortion on the order of the two d-to-d bands can be in turn correlated to the split of the $d\pi$ orbitals. For a polar compression, as shown in Scheme 2, the $d\pi(a_1)$ orbital concentrated along the C_3 axis might undergo more destabilization leading to the orbital energy sequence $\varepsilon(a_1) > \varepsilon(e)$. Thus, the A_2 band, arising from the pure $d\pi(e) \rightarrow d\sigma(e)$ one-electron excitation, will clearly have a higher energy than the E band which is a mixture of the $d\pi(e) \rightarrow d\sigma(e)$ and $d\pi(a_1) \rightarrow d\sigma(e)$ one-electron excitations. For Λ-$[M(en)_3]^{3+}$ (M = Co, Cr) that both have an azimuthal contraction and a polar compression, we see that, in line with the general rule, the E(d-d) and A_2(d-d) bands are respectively positive and negative with the energy order of $\upsilon(E) < \upsilon(A_2)$ (Figure 2), while the E(LMCT) and A_2(LMCT) bands exhibit opposite sign patterns.

Formally, d-to-d transitions are symmetry forbidden. However, we have shown in previous studies[12,45] that the d-to-d transitions gain their CD activity from an azimuthal distortion away from O_h symmetry of the six nitrogen atoms coordinated to the metal. The same distortion is responsible for the CD activity of LMCT transitions that are magnetically forbidden under O_h symmetry.

3.2. Complexes with Unsaturated Ligands. Cr(acac)$_3$. The MO diagrams for $Cr(acac)_3$ and $Co(acac)_3$ share very similar features (Figure 3); the six occupied ligand-based σ-type MOs $e_g(e)$, $a_{1g}(1a_1)$ and $t_{1u}(2e, 1a_1)$ and one set of the occupied ligand-based π-combinations ($2a_2$, 3e) are stabilized and situated below the metal t_{2g} MOs. Similar to the amine compounds, the empty $d\sigma$ orbitals are more destabilized for Cr(III) than Co(III) because of the stronger metal−ligand σ-interaction. In fact for Cr(III) they appear above the empty ligand-based π^* MOs.

The simulated and experimental CD spectra for $Cr(acac)_3$[43] and $Co(acac)_3$[52] are shown in Figure 5a and 5b, respectively.

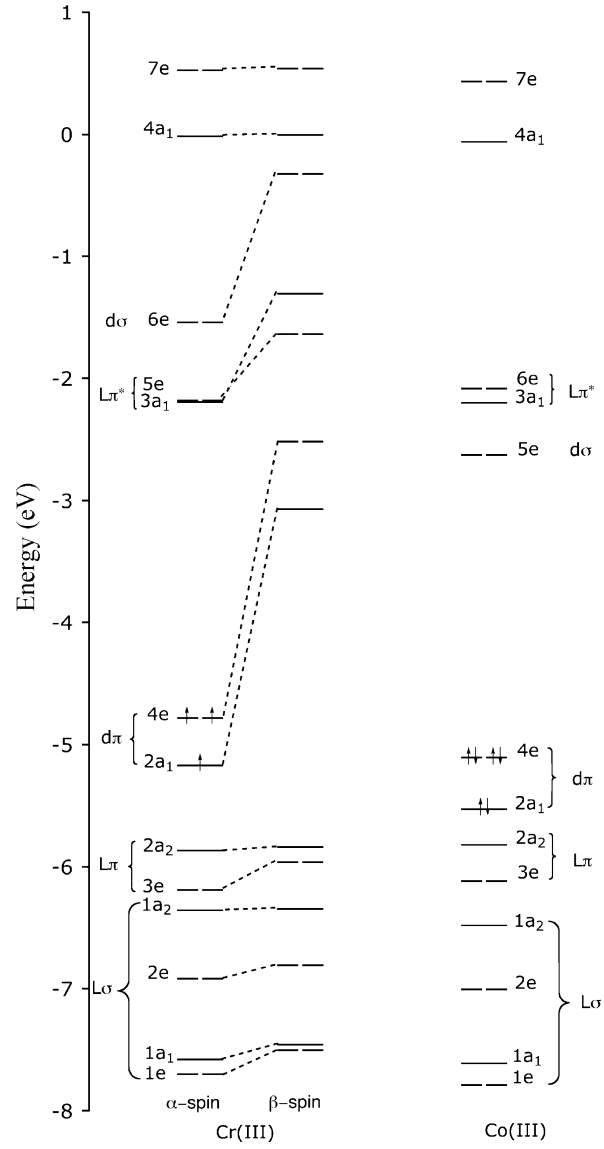

Figure 3. Molecular orbital diagram for $M(acac)_3$ (M = Cr, Co). In the Cr(III) case, the levels on the left are α-spin orbitals and those on the right are β-spin orbitals. Orbitals with no character indicated refer to bonded σ-orbitals of ligand.

Our DFT calculations yield for $Co(acac)_3$ at low energy two d-to-d excitations $4(A_2)$ and 5(E). Here, $4(A_2)$ gives rise to a negative CD band A whereas 5(E) yields a positive band B. The two simulated bands A and B are assigned to I and II, respectively, in the experimental spectrum. The same two excited states $4(A_2)$ and 5(E) are found at somewhat higher energy in the simulated spectrum of $Cr(acac)_3$ where they appear as part of band B. The higher energy of the d-to-d transition for Cr(III) compared with Co(III) is due to the corresponding larger crystal field splitting, Figure 3. We assign for $Cr(acac)_3$ band B to II in the corresponding experimental CD spectrum. We notice that in both acac systems the two d-to-d bands show the same sign pattern as that for $[M(en)_3]^{3+}$, although the azimuthal distortions now have the opposite sign with $\Delta\phi = +2.5°$ for $Cr(acac)_3$ and $\Delta\phi = +9.3°$ for $Co(acac)_3$ in comparison with $\Delta\phi = -7.1°$ for $[Cr(en)_3]^{3+}$ and $\Delta\phi = -6.3°$ for $[Co(en)_3]^{3+}$. This is probably because (1) the general rule was proposed based

(52) Von Dreele, R. B.; Fay, R. C. *J. Am. Chem. Soc.* **1971**, 4936–4938.

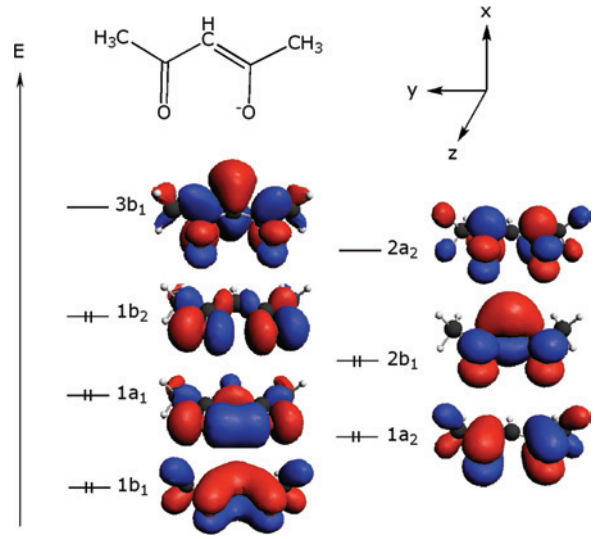

Figure 4. Frontier MOs in Free acac.

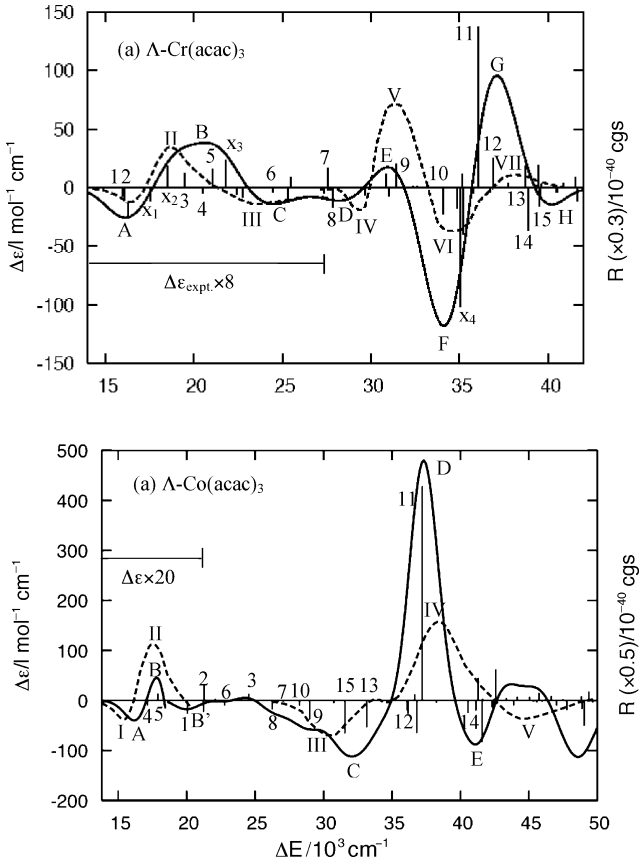

Figure 5. (a) Simulated (solid line) and experimental[43] (dashed line) CD spectra for Λ-Cr(acac)$_3$ in ethanol. The low energy part of the experimental spectrum is magnified by a factor of 8. A global red-shift of -5.0×10^3 cm^{-1} has been applied to the computed excitation energies; (b) simulated (solid line) and experimental[51] (dashed line) CD spectra for Λ-Co(acac)$_3$ in ethanol. A global red-shift of -4.0×10^3 cm^{-1} has been applied to the computed excitation energies. See also the caption for Figure 2.

on σ-bonded complexes[45] while in π-bonded systems, ligand π-orbitals could also make a contributions to the rotatory strengths; and (2) even if for σ-bonded complexes, the two bands do not change their signs exactly at an azimuthal angle of 60°. On the other hand, the order of A_2 and E has changed as expected from υ(E) < υ(A_2) in $[M(en)_3]^{3+}$ to υ(E) > υ(A_2)

Table 2. Spectral Properties for Λ-Cr(acac)$_3$

no.	R^a (10^{-40} cgs)	ΔE^b (10^3 cm^{-1})	symmetry[c]	one-electron excitation[d] MO→MO	%
1	−25.49	20.96	E	α: 4e → 3a$_1$	82
				α: 4e → 5e	13
2	−33.37	21.10	E	α: 4e → 5e	83
				α: 4e → 3a$_1$	15
x$_1$	−40.06	22.57	A_2	β: 2a$_2$ → 2a$_1$	89
x$_2$	+59.80	23.53	E	β: 3e → 2a$_1$	92
3	+39.98	24.49	E	α: 2a$_1$ → 5e	97
4	−14.86	25.48	A_2	α: 4e → 6e	98
5	+52.44	26.05	E	α: 4e → 6e	89
				α: 2a$_1$ → 6e	6
x$_3$	+77.18	26.80	E	β: 2a$_2$ → 4e	79
6	−12.64	29.44	E	α: 2a$_1$ → 6e	66
				β: 2e → 2a$_1$	27
7	+56.28	32.56	E	β: 2a$_2$ → 5e	32
				α: 3e → 5e	23
				α: 3e → 3a$_1$	21
8	−56.73	32.82	A_2	α: 3e → 5e	46
				β: 3e → 5e	37
9	+66.48	36.44	E	β: 3e → 3a$_1$	50
				β: 3e → 5e	22
10	−74.89	39.08	E	α: 1a$_2$ → 6e	78
				β: 3e → 3a$_1$	6
x$_4$	−339.89	40.01	A_2	β: 1e → 4e	39
				β: 2a$_2$ → 3a$_1$	14
				β: 3e → 5e	11
11	+459.10	41.06	E	β: 3e → 3a$_1$	20
				α: 1a$_2$ → 6e	13
				β: 2e → 5e	11
12	+83.31	41.90	E	β: 2e → 5e	85
13	+60.34	43.73	E	α: 2e → 6e	57
				α: 1a$_1$ → 5e	13
14	−121.91	43.88	E	α: 1a$_1$ → 5e	39
				α: 2e → 6e	19
15	−52.65	44.51	A_2	α: 2e → 6e	55
				α: 1e → 5e	16

[a] Rotatory strength; for the degenerate E states the rotatory strength given is the sum of the contribution from E_x and E_y. [b] Excitation energy. [c] Symmetry of the excited state. [d] Major contributions from one electron excitations to the transition.

in M(acac)$_3$ as the polar distortion changes from compression to elongation and the dπ(a$_1$) orbital now lies lower than the dπ(e). It is worth to note that the metal−ligand π-interactions in this case act to enhance the effect of the polar distortion and result in a more noticeable trigonal splitting in comparison with that of the other systems studied here. The highest occupied π MO on single acac ligand is 2b$_1$ (C_{2v}) as shown in Figure 4. The symmetry Lπ combinations made up of this orbital have two e-components that are able to destabilize the dπ(e) orbitals and one a_2-component that is unable to interact with either the dπ(e) or dπ(a$_1$) because of symmetry. Such an interaction causes a splitting of the dπ-set with the e-levels of higher energy than the a$_1$. There is also an Lπ*-set available for interaction with dπ. This set is made up of empty single-ligand orbitals designated 2a$_2$ in Figure 4. The Lπ*-combinations span the e and a$_1$ representations. As a consequence, both the dπ(e) and dπ(a$_1$) can interact with Lπ*. It is thus not expected that the interaction between Lπ* and dπ will add much to the dπ(e)/dπ(a$_1$) splitting.

The stronger crystal field splitting in Cr(III) pushes dσ(6e) above the 3a$_1$ and 5e Lπ* levels, Figure 3. The first two transitions in Cr(acac)$_3$ named 1(E) and 2(E) of Table 2 and Figure 5a are as a result made up of metal-to-ligand charge

transfer (MLCT) excitations. Here, 1(E) is represented by the $d\pi(4e) \rightarrow L\pi^*(3a_1)$ one-electron excitation and 2(E) by the $d\pi(4e) \rightarrow L\pi^*(5e)$ excitation. The two transitions both have negative rotatory strengths and give rise to one negative CD band marked "A" in the simulated spectrum. We assign A to band I of the experimental CD spectrum for $Cr(acac)_3$. We note that 1(E) and 2(E) in the Co(III) system is making up the likewise negative CD band B′. The two transitions are of higher energy in the Co(III) complex because of the smaller $\langle d\pi|L\pi\rangle$ overlaps for Co(III) than for Cr(III), just as in the case of the corresponding $\langle d\sigma|L\sigma\rangle$ overlaps.

The last of the $d\pi \rightarrow L\pi^*$ MLCT transitions is 3(E). It is found at lower energy in $Cr(acac)_3$ as part of band B and at higher energy in $Co(acac)_3$. The transition is ascribed to the $d\pi(2a_1) \rightarrow L\pi^*(5e)$ excitation and has a higher energy than 1(E) and 2(E) because of the $d\pi$ splitting. It gives rise for both systems to a positive rotatory strength. We have finally at low energy for Cr(III) three transitions $x_1(A_2)$, $x_2(E)$, and $x_3(E)$ that are not possible for $Co(acac)_3$, Table 2 and Figure 5. They involve one-electron excitations from $L\pi(2a_2, 3e)$ to the empty $d\pi$ levels. All three π-ligand to $d\pi$-metal CT transitions are part of band B in the simulated spectrum that we assign to band II in the corresponding experimental spectrum. Furthermore, the excitation 6 in both compounds is assigned to the E component of the formally electric and magnetic forbidden d-to-d transitions of respectively $A_{2g}{}^4 \rightarrow T_{1g}{}^4$ (Cr(III)) and $A_{1g}{}^1 \rightarrow T_{2g}{}^1$ (Co(III)) O_h parentage. In $Cr(acac)_3$, it has a contribution to the simulated band C that can be assigned to band III of the experimental spectrum.

The high energy region ($>25 \times 10^3$ cm^{-1}) of the two CD spectra in Figure 5 is dominated by charge transfer and internal ligand excitations. In fact there is a considerable mixing of the two types of one-electron excitations within the same state-to-state transitions. The most intense CD bands V and VI in the experimental spectrum of $Cr(acac)_3$ were assigned[41] to local $\pi \rightarrow \pi^*$ ligand excitations corresponding to $A_2{}^4 \rightarrow E^4$ and $A_2{}^4 \rightarrow A_1{}^4$ transitions, respectively. In partial agreement with this assignment, our computations yield two bands, E and F, because of similar transitions. Here, the transition 9(E) responsible for band E/V is mainly ascribed to the $\pi \rightarrow \pi^*$ excitations. However, for transition $x_4(A_2)$ responsible for band F/VI, there is a strong mixing of contributions from LMCT (39%) as well as $\pi \rightarrow \pi^*$ excitations (25% in total), Table 2. The intense simulated band G results mainly from excitation 11 that is predominately made up of CT and internal ligand $\pi \rightarrow \pi^*$ and $\sigma \rightarrow \pi^*$ one-electron excitations, Table 2. Band D contains in addition transitions 12(E) and 13(E) made up of $\sigma \rightarrow \pi^*$ and $\sigma \rightarrow d\sigma$ excitations, respectively. We assign band G to the much weaker experimental band VII for which no assignment was made in the original experimental paper.[43] Considering the assignment and the sign of the rotatory strengths for bands F, G and H of the simulated spectrum of $Cr(acac)_3$, they are related respectively to bands C, D, and E in the cobalt system. Band D in Co(III) exhibits an extremely high intensity as it has a major LMCT character that is formally allowed. It is not surprising that excitations 7, 8, 9, 12, and 14, mainly localized on the acac ligand, are situated at similar positions in the simulated bar spectra of Co(III) and Cr(III), Figure 5. On the other hand, transitions that have dominant $L\sigma$-to-$d\sigma$ contribution, for instance, 10, 13, and 15 occur at much lower energy for Co(III) than for Cr(III) because of the smaller crystal field splitting in the Co(III) system.

As we mentioned earlier, the qualitative analysis given previously[12,45] for $[Co(en)_3]^{3+}$ leads to the prediction that the E and A_2 components of the $L\sigma \rightarrow d\sigma$ CT excitations should exhibit opposite sign pattern with respect to the d-to-d analogues. This has been shown to be the case in $[M(en)_3]^{3+}$ (M = Cr, Co). For the Λ-acac complexes, $4(A_2)$ and 5(E) corresponding to d-to-d transitions have respectively negative and positive rotatory strengths, Table 2. We find that 10(E) with a large $L\sigma \rightarrow d\sigma$ contribution is opposite in sign to 5(E), Table 2. However, the $A_2(15)$ component with the largest $L\sigma \rightarrow d\sigma$ contribution has the same sign as $4(A_2)$ because of participations from $L\sigma \rightarrow L\pi^*$ and $L\pi \rightarrow L\pi^*$ excitations which are not considered in the qualitative analysis[12,45] based on σ-bonded diamine complexes.

$[Cr(Thiox)_3]^{3-}$. Although there have been many studies on absorption spectra of complexes with sulfur containing ligands, few have dealt with dithiooxalate complexes and the interpretation of their spectra. It was demonstrated[44] in the few available experimental studies that CD data can be very useful for identifying individual absorption components in the absorption spectra of dithiooxalate complexes. Otherwise the interpretation of their absorption spectra can be difficult because of the presence of overlap between the broad, intense bands in the visible region with the intense near-ultraviolet absorption bands from ligand-to-ligand transitions. We report here the computed CD spectra of $[M(Thiox)_3]^{3-}$ (M = Cr, Co, Table 3) and compare them with the available experimental data. For the Cr(III) system, no quantitative CD spectrum has been reported since the highly soluble $[Cr(Thiox)_3]^{3-}$ anions undergo rapid racemization.[44] In this case, only qualitative CD measurements were possible.

As shown in Figure 6, the two simulated CD spectra exhibit quite similar features in the whole energy region. The lowest part of both spectra is dominated by $d\pi \rightarrow L\pi^*$ excitations (1 and 2) that give rise to band A. They occur at quite low energy, in the region of 10 to 15 $\times$ 10^3 cm^{-1} because in both compounds the LUMOs are now made up of empty ligand π^*-combinations that are situated rather close to the $d\pi$ levels (Figure 7) in comparison with the corresponding orbitals in the acac systems of Figure 3. Experimentally, the limited range of the dichrograph prevented the investigation of this region.

The typical d-to-d transitions, $A_2(3)$ and E(4) in Figure 6, are predicted to be respectively negative and positive. Both systems show an azimuthal contraction, and the sign pattern of the two excitations appears to follow the general rule. Interestingly, both complex ions have the same elongated polar distortion with $s/h = 1.19$. The $d\pi$ set splits with expected energy sequence in view of the polar distortion. In

Table 3. Spectral Properties for Λ-$[Cr(Thiox)_3]^{3-}$

no.	R^a (10^{-40} cgs)	ΔE^b (10^3 cm^{-1})	symmetry[c]	one-electron excitation[d] MO→MO	%
1	+10.91	14.00	E	α: 7e → $4a_2$	93
2	−22.18	14.99	E	α: 7e → 8e	91
3	−32.80	21.49	A_2	α: 7e → 9e	91
4	+51.62	21.75	E	α: 7e → 9e	67
				α: $4a_1$ → 9e	13
5	+43.06	22.17	E	β: 6e → $4a_2$	20
				α: 6e → $4a_2$	20
				α: $3a_2$ → 8e	20
x_1	+29.82	24.39	E	β: 6e → $4a_1$	52
				β: 5e → $4a_2$	13
x_2	−55.20	24.81	E	β: $2a_2$ → 7e	28
				β: 5e → $4a_1$	18
				β: 6e → $4a_1$	16
x_3	+42.46	25.62	E	β: 5e → $4a_1$	68
				α: $2a_2$ → 8e	11
6	−69.41	27.30	E	α: $2a_2$ → 8e	62
				β: $3a_2$ → 8e	10
7	−32.54	30.65	E	α: 5e → 9e	70
x_4	−27.76	30.98	E	β: 2e → 7e	63
				α: 3e → $4a_2$	10
8	−49.08	32.80	A_2	α: $2a_1$ → $4a_2$	53
				β: 5e → 8e	10
9	+39.25	33.53	E	β: 4e → 8e	66
10	−34.01	34.13	E	α: $2a_2$ → 9e	83
11	+20.39	34.36	E	β: 1e → $4a_2$	35
				α: $1a_2$ → 8e	27
				α: 1e → $4a_2$	16
12	+40.38	35.23	E	β: 1e → $4a_2$	35
				α: 2e → 8e	30
				α: 2e → $4a_2$	13
13	+52.59	36.15	E	β: $2a_1$ → 8e	34
				α: 2e → 8e	15
				α: 2e → $4a_2$	12
14	+81.23	39.03	E	α: $4a_1$ → 10e	67
15	−67.99	40.52	E	α: 3e → 9e	52
				β: 1e → 8e	22
16	+29.90	40.57	A_2	α: 3e → 9e	47
				β: 1e → 8e	30
17	+34.58	41.12	E	β: 1e → 8e	53
				α: $1a_2$ → 9e	31
18	−70.30	41.23	A_2	β: 1e → 8e	63
				α: 3e → 9e	18

[a] Rotatory strength; for the degenerate E states the rotatory strength given is the sum of the contribution from E_x and E_y. [b] Excitation energy. [c] Symmetry of the excited state. [d] Major contributions from one electron excitations to the transition.

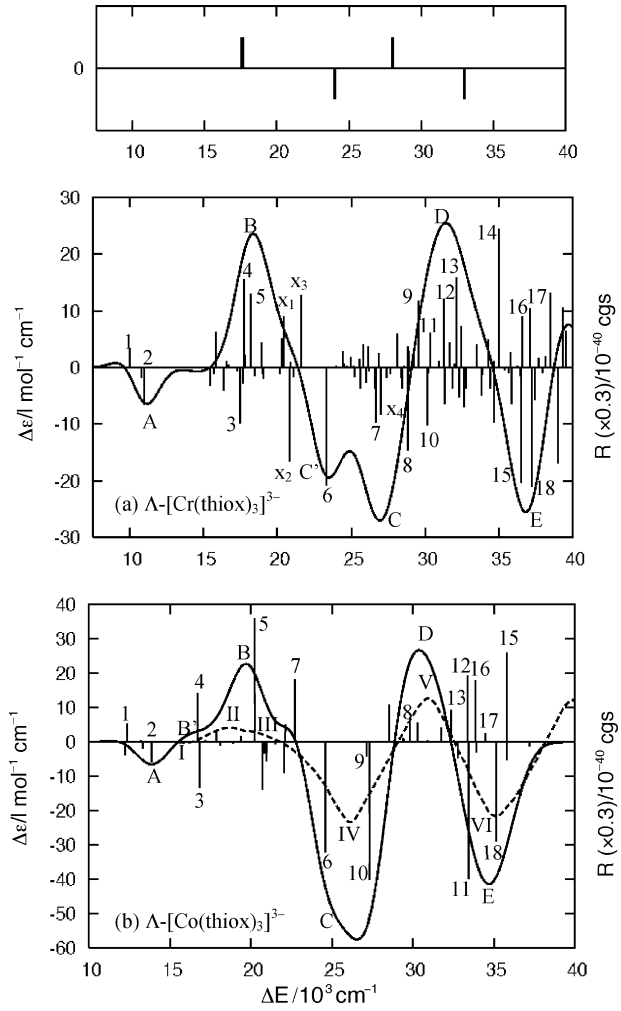

Figure 6. (a) Simulated CD spectra for Λ-$[Cr(Thiox)_3]^{3-}$. Experimental CD from qualitative measurements[44] is shown by the bar spectrum. (b) Simulated (solid line) and experimental[44] (dashed line) CD spectra for Λ-$[Co(Thiox)_3]^{3-}$. A global red-shift of -4.0×10^3 cm^{-1} has been applied to the computed excitation energies of both compounds. Theoretical excitation energies and rotatory strengths are indicated by bars. See also the caption for Figure 2.

$[Cr(Thiox)_3]^{3-}$, the dπ-levels show an obvious split because of a similar enhancing effect of metal−ligand π-interaction as discussed for $M(acac)_3$, and the order of the two excitations appears to be in agreement with the qualitative rule based in Scheme 2. Meanwhile, the two d-to-d components in $[Co(Thiox)_3]^{3-}$ are very close in energy since the dπ-orbitals in this case are almost degenerate, Figure 7. The E component nevertheless occurs at a little bit lower in energy although the dπ(e) level is slightly higher than the dπ(a_1) level. For the Cr(III) system, the two d-to-d excitations, together with an internal ligand $\sigma \rightarrow \pi^*$ excitation (5) in the same region, contribute largely to generate a single positive band B. The qualitative experimental CD curve[44] for $(-)_{546}$-KCa$[Cr(Thiox)_3]$ shows in this region a positive peak (17,600 cm^{-1}) that was assigned to the d-to-d E band. It was accordingly assumed that the A_2 component should be present at lower frequency in a region outside of the range of the measurement. The two d-to-d excitations in $[Co(Thiox)_3]^{3-}$ appear as a shoulder B′, and the ligand-localized excitation 5 yields a band (B) comparable to that in the Cr(III) system. In the experimental spectrum of $[Co(Thiox)_3]^{3-}$, bands I, II, and III were previously[44] assigned to the $A_2(A_{1g}{}^1 \rightarrow T_{1g}{}^1)$, $1E(A_{1g}{}^1 \rightarrow T_{1g}{}^1)$, and $2E(A_{1g}{}^1 \rightarrow T_{2g}{}^1)$ d-to-d components, respectively. Based on our calculations, however, we would like to correlate these bands to A, B′, and B.

The region beyond 22×10^3 cm^{-1} of both CD spectra can be mainly ascribed to internal ligand transitions, although there are to some extent contributions from CT excitations. A good correlation is achieved between theory and experiment. Thus, the simulated bands C, D, and E of Co(III) after a red-shift of 4×10^3 cm^{-1} accord well with the observed bands IV, V, and VI. On the other hand, the CD of Cr(III) appears in line with the qualitative curve of $(-)_{546}$-$[Cr(Thiox)_3]^{3-}$ which also shows CD bands [(−) at ca. 24,000, (+) at ca. 28,000, and (−) at ca. 33,000 cm^{-1}] similar to those of the Co(III) complex in this region.[44] It is seen from Figure 6a that the simulated bar spectrum of Cr(III)

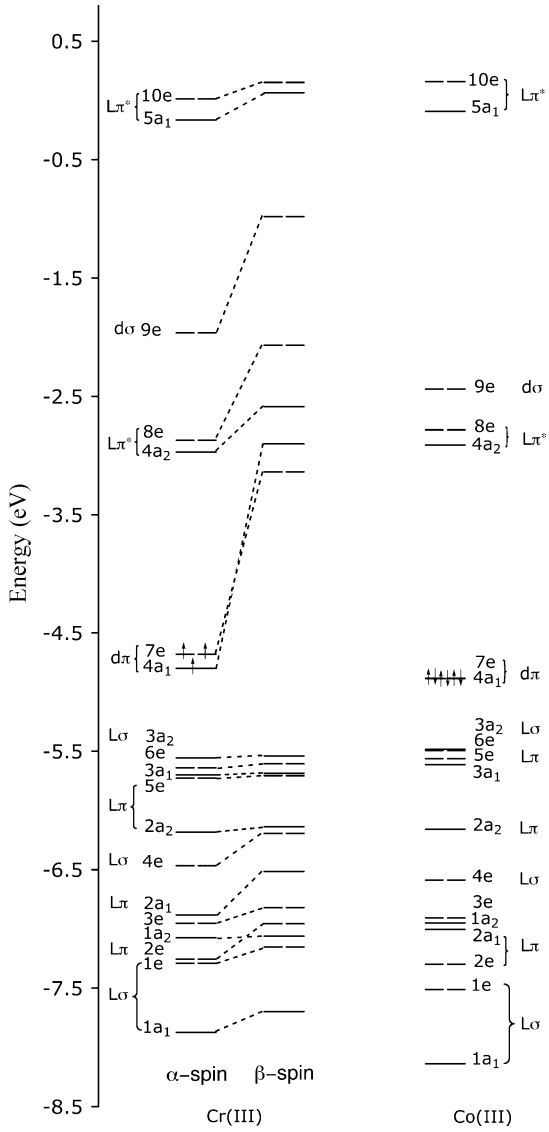

Figure 7. Molecular orbital diagram for $[M(Thiox)_3]^{3-}$ (M = Cr, Co). In the Cr(III) case, the levels on the left are α-spin orbitals and those on the right are β-spin orbitals. Orbitals with no character indicated refer to bonded σ-orbitals of ligand.

exhibits far more excitations than the corresponding spectrum for the Co(III) system, which is mainly due to the excitations to the half-filled dπ orbitals from occupied ligand orbitals. In Figure 6a we number only excitations of major importance to the CD of Cr(III).

We notice again, that the predominant ligand-to-metal(dσ) excitations, for example, 7 and 10, have undergone a noticeable red-shift from Cr(III) to Co(III). The intense metal-to-ligand(Lπ*) CT excitation 14 ($4a_1 \rightarrow 10e$) in Cr(III) is situated at a similar absorption energy in Co(III), but it has too low intensity to be seen in the bar spectrum. There are in addition four ligand-to-metal(dπ) excitations of moderate intensity which are not possible for Co(III) and are therefore denoted by "x". They do not introduce notable new features to the CD of Cr(III), except that the excitation x_2 (L$\pi \rightarrow$dπ) is responsible for yielding the small peak C′.

$[Cr(ox)_3]^{3-}$ and $[Cr(mal)_3]^{3-}$. McCaffery et al.[27] and Butler et al.[28] reported independently the observed CD spectrum of $[Cr(mal)_3]^{3-}$. While the CD data in the UV

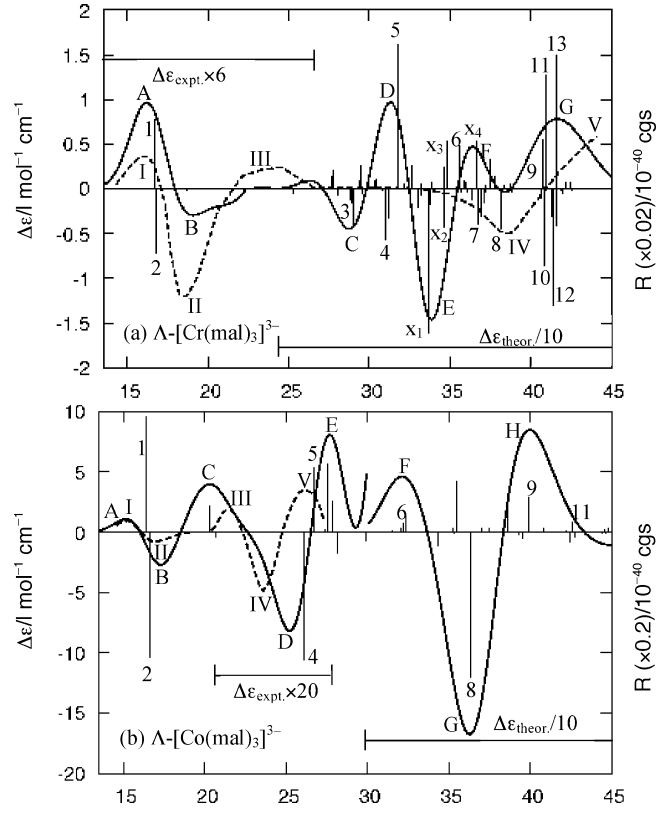

Figure 8. (a) Simulated (solid line) and experimental[27] (dashed line) CD spectra for Λ-$[Cr(mal)_3]^{3-}$. The low energy part of the experimental spectrum is magnified by a factor of 6, and the high energy part of the theoretical spectrum is reduced by a factor of 10; A global red-shift of -7.0×10^3 cm^{-1} has been applied to the computed excitation energies; (b) Simulated (solid line) and experimental[52] (dashed line) CD spectra for Λ-$[Co(mal)_3]^{3-}$; The high energy part of the experimental spectrum is magnified by a factor of 20 and that of the theory is reduced by a factor of 10; A global red-shift of -4.0×10^3 cm^{-1} has been applied to the computed excitation energies. See also the caption of Figure 2.

region are not available from the measurement by Butler et al., the spectra recorded by the two groups are very similar in the d-to-d transition region, indicating that the complex ion measured must in both cases have the same absolute configuration. However, the complex ion giving rise to the same d-to-d CD spectra by either study was assigned opposite absolute configurations by the two groups, based respectively on the assignment of the E component of the d-to-d transition[27] and an X-ray structure analysis.[28]

Our DFT simulations of the CD spectrum are based on the Λ enantiomer. This is also the configuration assigned by McCaffery et al. to their (-)-$[Cr(mal)_3]^{3-}$ sample. Figure 8a compares the simulated CD spectrum with experiment.[27] The bands A/I and B/II are assigned respectively to the E and A_2 components arising from the $A_{2g}{}^4 \rightarrow T_{2g}{}^4$ transitions. The $A_{2g}{}^4 \rightarrow T_{1g}{}^4$ d-to-d transition was assigned[27,28] to the experimental band III. Our calculated rotatory strength for this transition is too small to be noticed in the simulated spectrum. We point out that both the experimental and theoretical CD bands for $[Cr(mal)_3]^{3-}$ are very weak in the d-to-d region, Figure 9. The small optical activity was previously ascribed to the small azimuthal distortion[28] ($\Delta\phi$ = 0.2(5)°) away from the ideal octahedron value of ϕ = 60°. On the basis of our computations, however, the rotatory

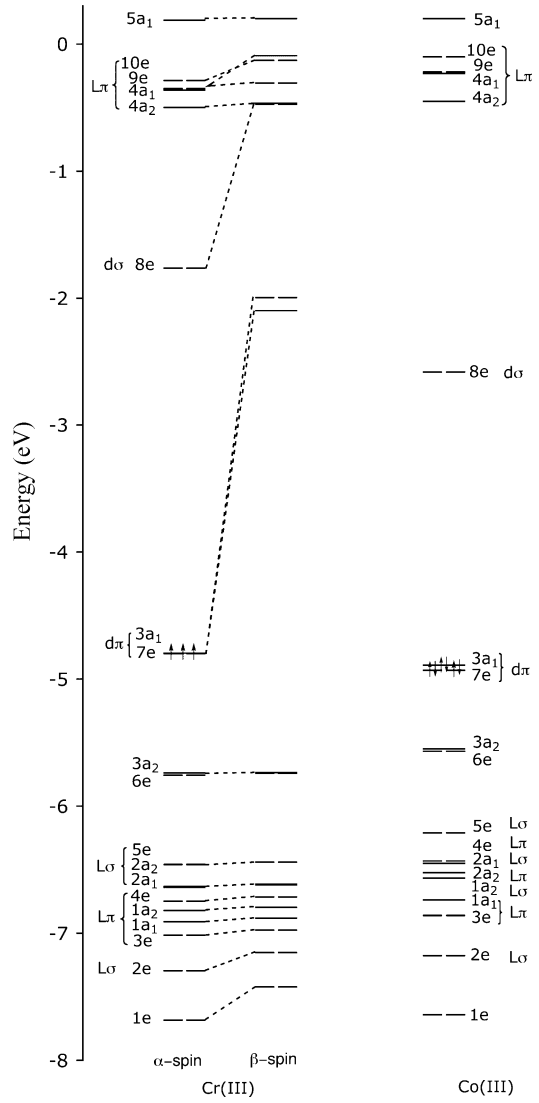

Figure 9. Molecular orbital diagram for $[M(mal)_3]^{3-}$ (M = Cr, Co). In the Cr(III) case, the levels on the left are α-spin orbitals and those on the right are β-spin orbitals. Orbitals with no character indicated refer to bonded ligand σ-orbitals.

strengths are of the same order as those in other Cr(III) complexes studied here. The corresponding azimuthal angle obtained from our DFT geometry optimization is 62.0°. We then suggest that the weak CD of $[Cr(mal)_3]^{3-}$ in this region is mainly due to the substantial cancelation of the A_2 and E components owing to their small splitting ($\upsilon(E) - \upsilon(A_2) = -40\ cm^{-1}$) and the comparable absolute value of the rotatory strengths of the two excitations (1 and 2 of Table 4). The splitting is expected to be very small because the calculated polar distortion parameter *s*/*h* of 1.21 is very close to the value of 1.22 appropriate for ideal octahedral coordination. The corresponding CD bands for the d-to-d transition in the Co(III) system with the same configuration, A/I and B/II of Figure 8b, are more intense but otherwise similar. The geometric parameters for $[Co(mal)_3]^{3-}$ are 1.13 (*s*/*h*) and 68.8° (ϕ). We would like to note that DFT tends to overestimate the CD intensity, especially when metal d-orbitals are involved.[15,29] But since the overestimation is found basically for all the computations, the comparative analysis made here should be meaningful.

Table 4. Spectral Properties for Λ-$[Cr(mal)_3]^{3-}$

no.	R^a (10^{-40} cgs)	ΔE^b (10^3 cm^{-1})	symmetry[c]	one-electron excitation[d] MO→MO	%
1	+38.57	23.71	E	α: 7e → 8e	53
				α: $3a_1$ → 8e	46
2	−35.97	23.75	A_2	α: 7e → 8e	100
3	−21.28	35.98	E	α: 7e → 9e	70
				β: 5e → 7e	12
4	−27.82	38.02	E	α: 5e → 8e	88
5	+81.07	38.80	A_2	α: 5e → 8e	40
				β: 4e → 7e	26
				β: $1a_2$ → $3a_1$	25
x_1	−80.58	40.66	E	β: 3e → 7e	29
				α: $1a_2$ → 8e	25
				α: $2a_2$ → 8e	15
x_2	−21.52	41.62	A_2	β: 2e → 7e	86
x_3	+26.85	41.83	E	β: 2e → 7e	77
6	+24.37	42.63	A_2	α: 3e → 8e	70
				β: 6e → 8e	13
x_4	+27.01	43.64	E	β: 1e → 7e	87
7	−15.18	43.93	E	α: $3a_2$ → 10e	25
				β: $3a_2$ → 9e	25
				α: 6e → 10e	19
8	−22.01	45.18	E	α: 2e → 8e	65
9	+27.48	47.71	E	α: 1e → 8e	82
10	−42.41	47.87	A_2	β: $3a_2$ → $5a_1$	67
				α: $3a_2$ → $5a_1$	32
11	+63.34	47.96	E	α: 6e → $5a_1$	51
				β: 6e → $5a_1$	48
12	−64.70	48.39	E	β: 5e → 8e	71
13	+74.30	48.63	A_2	β: 5e → 8e	85

[a] Rotatory strength; for the degenerate E states the rotatory strength given is the sum of the contribution from E_x and E_y. [b] Excitation energy. [c] Symmetry of the excited state. [d] Major contributions from one-electron excitations to the transition.

Similar to the acac systems, the sign pattern of the two d-to-d bands in both complexes resemble again that in $[M(en)_3]^{3+}$ despite the change in the azimuthal distortion. The change in the polar distortion from compression for $[M(en)_3]^{3+}$ to elongation for $[M(mal)_3]^{3-}$, on the other hand, does not reverse the energy sequence of the two bands, Figure 8. The dπ split is rather small, especially in $[Cr(mal)_3]^{3-}$, with the e-levels situated slightly lower than the a_1 level, which is probably a result of the stabilization experienced by the e-orbitals from interacting with the Lπ* combinations.

We find as well that the low energy region of the CD spectrum for Λ-$[Cr(ox)_3]^{3-}$ (Table 5) contains two d-to-d transitions, 1 and 2 of Figure 10. Here, $1(A_2)$ and 2(E) originate again from $A_{2g}{}^4 \rightarrow T_{2g}{}^4$. The two transitions have merged into one band A because of the small separation between 1 and 2. We assign 1 to the observed band I and suggest that 2 in part is responsible for the experimental band II. The band A contains in addition the excitations 3(E) and in part 4(E). Here, 3 represents a MLCT excitation dπ (6e)→Lπ*($4a_2$) whereas 4 belongs to the $A_{2g}{}^4 \rightarrow T_{1g}{}^4$ d-to-d transition. The high energy tail of 4 manifests itself as a negative band B. We assign B to the experimental band III. The simulated CD spectrum for Λ-$[Co(ox)_3]^{3-}$ has also been studied computationally previously.[41] It reveals in the d-to-d region the $1(A_2)$ and 2(E) components analogous to those in Λ-$[Cr(ox)_3]^{3-}$. In view of their geometries, both complex ions show azimuthal contraction and polar compression. We see that their CD spectra exhibit a sign pattern of the two

Table 5. Spectral Properties for Λ-$[Cr(ox)_3]^{3-}$

no.	R^a (10^{-40} cgs)	ΔE^b (10^3 cm^{-1})	symmetry[c]	one-electron excitation[d] MO→MO	%
1	−26.86	21.26	A_2	α: 6e → 7e	100
2	+33.60	21.43	E	α: 6e → 7e	67
				α: $4a_1$ → 7e	33
3	+16.26	22.96	E	α: 6e → $4a_2$	94
4	−10.65	23.29	E	α: $4a_1$ → 7e	62
				α: 6e → 7e	30
x_1	−13.35	29.08	E	β: $3a_1$ → 6e	90
5	−11.84	30.39	A_2	α: 5e → 7e	98
6	−32.02	32.05	E	α: $3a_2$ → 7e	86
7	+12.83	34.60	A_2	α: 4e → 7e	98
x_2	+12.09	38.78	E	β: 3e → $4a_1$	83
8	−22.48	42.38	E	β: $3a_2$ → 8e	42
				α: 2e → 7e	14
				α: $2a_1$ → 8e	12
x_3	−13.10	43.95	E	β: 1e → $4a_1$	60
				β: 2e → $4a_1$	15
9	+66.77	45.09	A_2	α: 1e → 7e	48
				β: 4e → 8e	22

[a] Rotatory strength; for the degenerate E states the rotatory strength given is the sum of the contribution from E_x and E_y. [b] Excitation energy. [c] Symmetry of the excited state. [d] Major contributions from one-electron excitations to the transition.

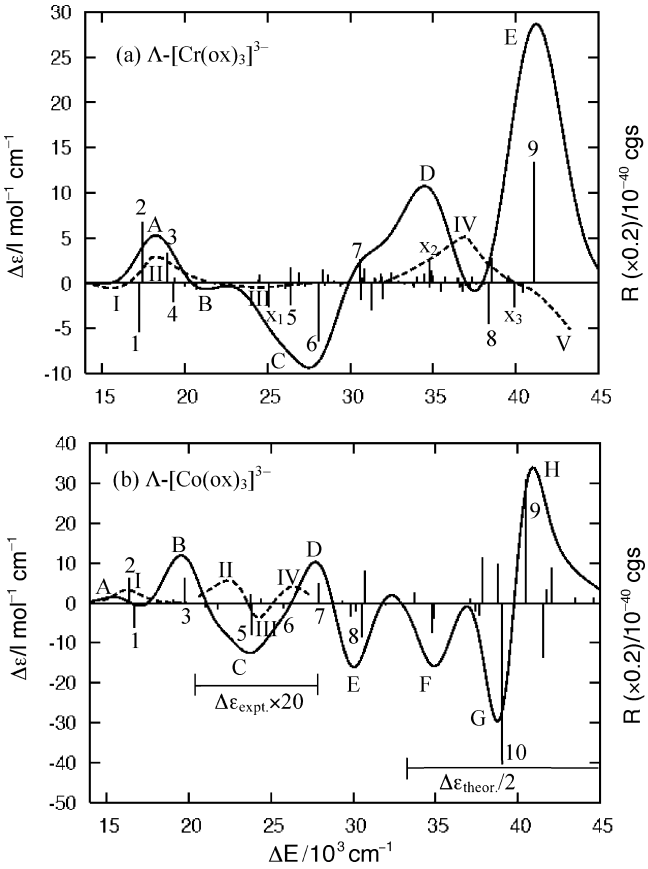

Figure 10. (a) Simulated (solid line) and experimental[27] (dashed line) CD spectra for Λ-$[Cr(ox)_3]^{3-}$. (b) Simulated (solid line) and experimental[52] (dashed line) CD spectra for Λ-$[Co(ox)_3]^{3-}$; the high energy part of the experimental spectrum is magnified by a factor of 20 and that of the theory is reduced by a factor of 2. A global red-shift of -4.0×10^3 cm^{-1} has been applied to the computed excitation energies of both compounds. See also the caption of Figure 2.

excitations as suggested by the rule with E being positive and A_2 negative. Whereas the two components in $[Co(ox)_3]^{3-}$ appears to have the expected energy sequence, a reversal is

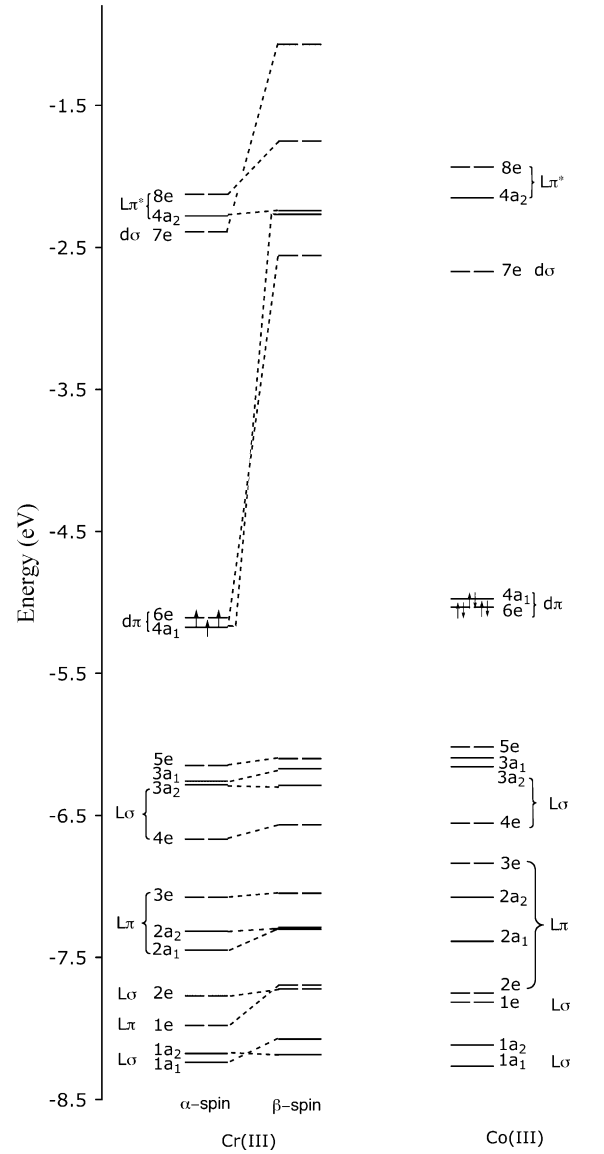

Figure 11. Molecular orbital diagram for $[M(ox)_3]^{3-}$ (M = Cr, Co). In the Cr(III) case, the levels on the left are α-spin orbitals and those on the right are β-spin orbitals. Orbitals with no character indicated refer to bonded ligand σ-orbitals.

shown by $[Cr(ox)_3]^{3-}$ both theoretically and experimentally, Figure 10. This might arise from the fact that while the polar compression tends to raise the $d\pi(a_1)$ orbital more in energy than the $d\pi(e)$ the opposing effect of the π-interactions between the $d\pi(e)$ and the ligand $L\pi$ combinations seems to overwhelm and raise the e-levels above the a_1 level. Accordingly, the corresponding $L\pi$-orbitals, appearing as 1e in $[Cr(ox)_3]^{3-}$ of Figure 11, are more stabilized compared with the counterpart (2e) in $[Co(ox)_3]^{3-}$ that has a comparable polar distortion. It is noted again that the $L\pi$ combinations made up of the b_1 single ligand orbital cannot by symmetry interact with the $d\pi(a_1)$.

Experimental CD data in the high energy region for $[M(ox)_3]^{3-}$ and $[M(mal)_3]^{3-}$ is non-existing in the case of Co(III) and sparse for Cr(III) with two broad bands VI and V of opposite signs, Figure 8 and 10. Interestingly, whereas the bands VI and V are respectively negative and positive for $[Cr(mal)_3]^{3-}$ the opposite is the case for $[Cr(ox)_3]^{3-}$. The

change in the sign sequence of VI and V between the two systems augmented with a similar change for bands I and II in the d-to-d transition region might suggest that the recorded spectra for $[Cr(ox)_3]^{3-}$ and $[Cr(mal)_3]^{3-}$ correspond to complexes of opposite configurations. However, this suggestion seems to be ruled out by a single-crystal polarized absorption spectrum[27] of $[Cr(mal)_3]^{3-}$ according to which both complexes have the Λ-configuration. Also our calculations indicate that the change in the sign sequence of I and II in $[Cr(ox)_3]^{3-}$ is associated with a change in the energy order of the A_2 and E components from the d-to-d transition $A_{2g}{}^4 \rightarrow T_{2g}{}^4$, Scheme 1, as discussed earlier. We further note that the excitations 6 and 7 in $[Cr(ox)_3]^{3-}$ and 4 and 5 in $[Cr(mal)_3]^{3-}$, which contribute largely to the bands C and D in both CD spectra, are assigned respectively to the E and A_2 components of the typical $A_{2g}{}^4 \rightarrow T_{2u}{}^4$ charge transfer. They have, as expected from the previous studies[12,45] based on molecular orbital theory, opposite signs with respect to the counterparts of the $A_{2g}{}^4 \rightarrow T_{2g}{}^4$ d-to-d transitions. We therefore suggest that these first two bands (C and D) in both systems are correlated to the corresponding experimental peaks IV and V, Figures 8 and 10. The simulations appear in line with the experiment for $[Cr(mal)_3]^{3-}$, while such a correlation for $[Cr(ox)_3]^{3-}$ yields a reverse sign pattern of the CD bands with respect to the measurement. At this point, we also see for the two complex ions that the computed CT excitations after a global red-shift are too low in energy compared to experiment. It has been shown that standard nonhybrid functionals tend to overestimate the HOMO−LUMO gap in 3d metal complexes and consequently yield too high d-to-d excitation energies. However, it appears less certain to address the systematic errors for the higher energy region dominated by charge transfer and/or internal ligand transitions. The errors may be caused by many factors, such as deficiencies in the density functionals, incomplete treatment of solvent effects, neglect of the presence of the counterion, and so forth.[15]

As for the origin of the CD in the complexes containing unsaturated ligands, we have elucidated in previous investigations[41,45] the mechanism by which typical charge transfer and ligand-localized transitions acquire optical activity. The contribution to the rotatory strengths associated with different transitions is interpreted in terms of transition moments of the type $\langle L\pi|\hat{\mathbf{o}}|L\pi^*\rangle$, $\langle L\sigma|\hat{\mathbf{o}}|L\pi^*\rangle$, or $\langle L\sigma|\hat{\mathbf{o}}|L\sigma^*\rangle$, and so forth within a single ligand.

4. Conclusion

In this work we have presented spin-unrestricted TD-DFT calculations on the electronic CD spectra of some open-shell $[Cr(L\text{-}L)_3]^{n+}$ complexes that involve both saturated and unsaturated bidentate ligands. The CD spectra of the Cr(III) systems are analyzed and correlated to the Co(III) analogues where data are available for both systems. In general, the $d\pi$-$d\sigma$ gap or crystal field splitting in the Cr(III) complexes appears larger than that in the Co(III) systems because of stronger interactions (overlaps) between the more diffused d-orbitals in Cr(III) and the ligand σ-orbitals in line with expectations. As a consequence, the d-to-d, as well as the LMCT, transitions occur at relatively higher energy in the Cr(III) systems.

Table 6. Relationship between CD of the $A_{2g}{}^4 \rightarrow T_{2g}{}^4(d^3)$ or $A_{1g}{}^1 \rightarrow T_{1g}{}^1$ (d^6) d-to-d Transitions and Geometry of Λ-$[M(L\text{-}L)_3]^{n+}$ Complexes

L−L	M	R(E)[a]	$\Delta\phi$ (deg)[b]	v(E-A_2)[c]	s/h[d]
en	Cr	+	−7.1	−	1.38
	Co	+	−6.3	−	1.28
acac	Cr	+	+2.5	+	1.19
	Co	+	+9.3	+	1.12
Thiox	Cr	+	−12	+	1.19
	Co	+	−5.6	−	1.19
mal	Cr	+	+2	−	1.21
	Co	+	+8.8	−	1.13
ox	Cr	+	−10.9	+	1.33
	Co	+	−3.8	−	1.29

[a] Sign of rotatory strength of the E symmetry. [b] Azimuthal distortion; $\phi = 60°$ for ideal octahedrons. [c] Trigonal splitting of the T_{1g} state. [d] Polar distortion; $s/h = 1.22$ for ideal octahedrons.

For trigonal dihedral d^3 complexes $[M(L\text{-}L)_3]^{n+}$ of bidentate ligands (L-L) where only σ-orbitals are involved, one finds that either the low energy or the high energy end of their CD spectra can be used to assign an absolute configuration. The low energy end is dominated by the $A_{2g}{}^4 \rightarrow T_{2g}{}^4$ d-to-d transitions that are split in D_3 symmetry into E(d-d) and A_1(d-d) components with E(d-d) of lower energy, Scheme 1. The high energy region is dominated by $A_{2g}{}^4 \rightarrow T_{2u}{}^4$ LMCT transitions split by D_3 symmetry into E(LMCT) and A_1(LMCT) components with E(LMCT) of lower energy. Correlation between the geometry of the complexes and the signs and positions of the CD component indicates, for the Λ-configuration with an azimuthal contraction, as in $[Cr(en)_3]^{3+}$, that E(d-d) and A_1(d-d) should be respectively positive and negative whereas the E(LMCT) and A_1(LMCT) should be respectively negative and positive. All the signs should be reversed for an azimuthal expansion. Meanwhile, polar distortions determine the sign of the E-A_1 split. The same rules apply in similar d^6 complexes[45] with "A_1" replaced by "A_2". It is thus suggested that CD spectra can be used to assign absolute configurations of $[M(L\text{-}L)_3]^{n+}$ complexes involving pure σ-ligands, provided that their geometric parameters are known.

For the corresponding $[M(L\text{-}L)_3]^{n+}$ complexes with both π- and σ-orbitals, we found that the E(d-d) and A_2(d-d)/A_1(d-d) excited states tend to retain respectively the positive and negative sign for all the complexes of Λ-configuration studied, regardless of the sign change of the azimuthal distortion. They can thus be used to assign absolute configurations for $[M(L\text{-}L)_3]^{n+}$ complexes for ligands containing both π- and σ-orbitals, provided that an identification of the E and A components of the d-to-d transitions can be made. The spectral and structural information for the complexes investigated here is summarized in Table 6.

With σ/π ligands, polar distortions are no longer an unambiguous indicator for the sign of the E-A_2/A_1 splitting. Thus, a polar compression with $s/h > 1.22$ (or elongation with $s/h < 1.22$) does not necessarily give rise to a negative (or positive) $\Delta v(E - A_2)$ as it is usually the case for the σ-bonded diamine complexes. The metal−ligand π-interactions might play an important role here in determining the

order of E-A_2/A_1 states by affecting the trigonal split of the dπ HOMOs. In $[M(mal)_3]^{3-}$ (M = Cr, Co) and $[Cr(ox)_3]^{3-}$ that show a reverse order of E-A_2/A_1 in view of the polar distortion, the anomalous dπ splitting is ascribed to the fact that the dπ(e) components may undergo more destabilization/stabilization upon interacting with Lπ/Lπ* combinations of the right symmetry. The E(LMCT) and A_2(LMCT)/A_1(LMCT) bands for σ/π ligands can not be used to assign absolute configurations since their rotatory strengths might change sign because of contributions from internal ligand transitions. With these qualifications, we suggest that TD-DFT can server as a useful tool for the assignment and interpretation of the CD spectra of complexes containing unsaturated ligands.

Acknowledgment. This work has received financial support from the National Science and Engineering Research Council of Canada (NSERC). One of us (J.F.) acknowledges the financial support of Alberta Ingenuity Fund (AIF). J.A. is grateful for financial support of his research by the National Science Foundation. T.Z. would like to thank the Canadian Government for a Canada Research Chair.

IC801229C